



SPE 89343

Reservoir Simulation of CO₂ Storage in Deep Saline Aquifers

A. Kumar, M. Noh, G.A. Pope, K. Sepehrnoori, S. Bryant and L.W. Lake, The University of Texas at Austin
SPE Members

Copyright 2004, Society of Petroleum Engineers Inc.

This paper was prepared for presentation at the 2004 SPE/DOE Fourteenth Symposium on Improved Oil Recovery held in Tulsa, Oklahoma, U.S.A., 17–21 April 2004.

This paper was selected for presentation by an SPE Program Committee following review of information contained in a proposal submitted by the author(s). Contents of the paper, as presented, have not been reviewed by the Society of Petroleum Engineers and are subject to correction by the author(s). The material, as presented, does not necessarily reflect any position of the Society of Petroleum Engineers, its officers, or members. Papers presented at SPE meetings are subject to publication review by Editorial Committees of the Society of Petroleum Engineers. Electronic reproduction, distribution, or storage of any part of this paper for commercial purposes without the written consent of the Society of Petroleum Engineers is prohibited. Permission to reproduce in print is restricted to a proposal of not more than 300 words; illustrations may not be copied. The proposal must contain conspicuous acknowledgment of where and by whom the paper was presented. Write Librarian, SPE, P.O. Box 833836, Richardson, TX 75083-3836, U.S.A., fax 01-972-952-9435.

Abstract

We present the results of compositional reservoir simulation of a prototypical CO₂ sequestration project in a deep saline aquifer. The objective was to better understand and quantify estimates of the most important CO₂ storage mechanisms under realistic physical conditions. Simulations of a few decades of CO₂ injection followed by 10³ to 10⁵ years of natural gradient flow were done. The impact of several parameters was studied, including average permeability, the ratio of vertical to horizontal permeability, residual gas saturation, salinity, temperature, aquifer dip angle, permeability heterogeneity and mineralization. The storage of CO₂ in residual gas emerges as a potentially very significant issue meriting further study. Under some circumstances this form of immobile storage can be larger than storage in brine and minerals.

Introduction

Geological Storage

Geological sequestration of CO₂ is one of the few ways to remove combustion emissions in sufficient volumes¹ to mitigate the greenhouse effect. Several groups have reported aquifer-scale simulations of the storage process, usually in order to estimate the volume that can be stored¹⁻¹⁴. Most schemes that have been put forward depend on storing CO₂ in the supercritical state. In these schemes, buoyancy forces will drive the injected CO₂ upward in the aquifer until a geological seal is reached. The permanence of this type of sequestration depends entirely on the integrity of the seal over very long periods of time. Assuring such integrity in advance is very difficult.

Our study focuses on three modes of CO₂ sequestration that avoid this concern: 1) **pore-level trapping** of the CO₂-rich gas phase within the geologic formation; 2) **dissolution into brine** in the aquifer; and 3) **precipitation** of dissolved

CO₂ as a mineral, e.g. calcite. All three modes are familiar, though to date the little attention has been paid to the first. Each of these modes is permanent for the time frame of interest in CO₂ sequestration. The key issues then become 1) how to maximize these three highly desirable forms of sequestration so that very large volumes of CO₂ can be permanently stored in aquifers, without the need for ensuring long-term seal integrity and 2) how long it takes for the injected CO₂ to migrate into these modes of storage.

The principal petrophysical parameters influencing storage as an immobile gas phase (in this paper, we use the term “gas” as shorthand for “supercritical fluid”) are relative permeability, including hysteresis, and the residual saturation of a nonwetting phase. Both depend on the rock making up the aquifer and thus can vary with location. The phase behavior of the CO₂/brine mixture controls storage in solution, and this depends upon brine salinity, temperature and pressure. The principal geochemical driver accompanying storage is the acidification of the brine resulting from dissociation of dissolved CO₂. Low pH brine¹⁰ in turn induces several reactions with minerals in the formation. An obvious example is the dissolution of carbonate cements. Other reactions are analogous to weathering, in which the acid extracts cations from aluminosilicates (feldspars, clays, etc.). The released cations may form relatively insoluble carbonate precipitates such as siderite. The competition between these reactions will determine the potential for additional storage by mineralization.

The time scales for these processes vary widely. Once CO₂ injection ends, the fluid displacement leading to residual saturations depends on absolute and relative permeabilities, hysteresis, buoyancy forces, the dip of the aquifer, the natural background flow gradient, and the magnitude of the residual saturation. Dissolution of CO₂ into brine is rapid, but the overall rate of mass transfer depends on contact between the phases. This is a complicated function of time, especially after injection stops, controlled by the same parameters as the post-injection fluid displacement. Geochemical reactions (mineral dissolution and precipitation) are typically slow^{1,10}, though under some conditions the rate may be comparable to other mass transport processes^{4,14}.

Approach

To study these processes, their dependence on aquifer parameters, and their characteristic time scales, we conducted a large set of two- and three-dimensional simulations with fully coupled reactive flow and transport. The Computer

Modeling Group's GEM simulator was used in this study⁸. Base case simulations were conducted for aquifer storage times of 1000 years. Some simulations were continued for up to 100,000 years.

Because this is a generic study of CO₂ storage in deep, saline aquifers rather than the study of a specific aquifer, the goal was to select representative characteristics for the aquifer as a base case for a systematic parameter study. This provides insight into the potential for CO₂ storage in forms that have minimal tendency to escape from the aquifer.

The input parameters for the base case simulation are summarized in Table 1. The simulated aquifer is 53,000 ft long, 53,000 ft wide and 1000 ft thick. Constant pressure wells are used along all boundaries to model an open aquifer, while the injector is in the center of the aquifer. The relative permeability curves are shown in Figure 3.

Pure supercritical CO₂ is injected into the aquifer for ten years. The injector is then shut in, and the simulation continues with only density differences driving the flow. Having established the base case, we conducted several simulations to study the effect of the parameters influencing the distribution of CO₂ in the aquifer. These parameters include permeability, the ratio of vertical to horizontal permeability, residual gas saturation, salinity, temperature and dip. Table 2 summarizes the different runs made. These runs did not include geochemical reactions.

This study assumed no conductive faults and no leaky wellbores in the aquifer. Such features would provide a potential escape route for mobile CO₂-rich gas. Their presence would not change our conclusions qualitatively, though they would certainly introduce a critical length scale – distance from injector to the potential leak – that would influence the design of strategies to permanently store CO₂.

Results and Discussion

Phase Behavior

The calibration of the fluid property models with experimental data is a very important first step in establishing the input to the simulator for this problem. CO₂ solubility is of obvious importance in evaluating storage in brine. Critical to evaluating the permanence of this mode of storage is the brine density: if it increases with CO₂ content, then it will sink relative to other fluid phases in the aquifer. Thus CO₂ solubility, brine density and brine viscosity models were calibrated against experimental data as a function of salinity, temperature and pressure. The brine density and viscosity also depend on the CO₂ concentration.

We made an extensive literature search to find the best sources of experimental data. Table 3 lists the different sources of solubility data for CO₂ in brine¹⁵⁻¹⁹. These sources give similar trends over a wide range of temperature and salinity

We tuned the Peng-Robinson equation-of-state²⁰⁻²¹ to fit available experimental data on the solubility of CO₂ in brine and the density of brine²²⁻²⁸ as a function of CO₂ concentration in the brine, brine salinity, temperature and pressure. Flash calculations are done in the compositional simulator each time step to calculate the phase behavior of the CO₂ and H₂O mixtures in each grid block as well as the density of both the gas and aqueous phases. The binary interaction parameter

between the CO₂ and H₂O was adjusted to fit the CO₂ solubility data and the volume shift parameter for H₂O was adjusted to fit the aqueous phase density. The computed curves for CO₂ solubility as a function of salinity and pressure are shown in Figure 1 along with selected experimental data points. Similar agreement occurred at temperatures ranging from 68 to 212 °F. Using the available solubility data, the binary interaction coefficient was correlated linearly with temperature and salinity for a temperature range of 68 to 212 °F and salinity range of 0 to 350,000 ppm of NaCl. We tuned the Pedersen correlation for brine viscosity²⁷.

Density data for pure water was taken from Wagner et al.²⁶ This source was preferred because it is based on the IAPWS-95 formulation adopted by International Association for the Properties of Water and Steam (IAPWS). Density data for pure brine have been taken from Simonson et al.²⁵ for a wide range of temperature (77–477 °F), pressure (1030–5830 psi) and salinity (30,000–300,000 ppm of NaCl). Unfortunately, there are very few experimental data in the temperature and pressure range of interest for the density of brine saturated with CO₂. Parkinson et al.²⁸ give density values for CO₂-H₂O mixtures for pressures less than 500 psia and temperatures less than 105 °F. Teng et al.¹⁸⁻¹⁹ give density values of CO₂-brine mixtures for temperatures less than 68°F. Data from Hnedkovsky et al.²⁴ were used to verify density trends. Those few density data that could be found were used to develop a correlation for the volume shift parameter of H₂O used in the Peng-Robinson EOS over the same range of temperature and salinity. Figure 2 shows an example of the predicted density of both brine and brine saturated with CO₂ as a function of salinity at 140 °F (60 °C) and 5830 psia. The density of brine saturated with CO₂ is slightly greater than that of brine without CO₂. However, the differences decrease as salinity increases.

Effect of aquifer properties

Table 2 summarizes the results when a wide range of aquifer properties were varied individually. Less CO₂ is stored in the ten-year injection period when the formation permeability is small. This is because the simulation includes a maximum bottom hole pressure for the injector, which limits its injection rate.

The effects of temperature and salinity reported in Table 2 reflect the changes in CO₂ solubility and in density of CO₂-saturated brine. The solubility of CO₂ in brine and the viscosity of brine both decrease with an increase in temperature. The former tends to lessen dissolution of CO₂ in brine, while latter increases the same due to increased contact of injected CO₂ with brine. The second phenomenon is more prominent since at higher temperatures a greater percentage of injected CO₂ goes into aqueous phase. Similarly smaller salinity corresponds to more dissolution because of increased solubility. Larger values for dip lead to greater lateral movement of CO₂, which in turn leads to increased dissolution. Although the horizontal to vertical permeability ratio (k_v/k_h) does not affect the distribution of CO₂ among phases significantly, it does affect spatial distribution. At small values of k_v/k_h , there is more horizontal movement of the CO₂ in the layers into which injection occurred. At larger values, there is more vertical migration followed by movement along the top seal.

Residual gas saturation has the greatest effect on the distribution of CO₂ among the three modes of storage (Figure 4). For small values of residual gas saturation, nearly 20% of the CO₂ is still mobile after 1000 years. Thus, there is greater movement of the CO₂-rich gas phase in the post-injection period. This increases the extent of contact between CO₂ and brine, which in turn leads to increased dissolution of CO₂ in brine. On the other hand, this also permits migration of CO₂ to the top seal of the aquifer. As illustrated later, it also leads to considerable migration along the top of the aquifer in the updip direction. In contrast, at larger values of residual gas saturation, most of the CO₂ is trapped as residual gas. There is correspondingly less CO₂ dissolved in brine. Most importantly, the amount of CO₂ that is still mobile after 1000 years is very small.

The strong influence of residual gas saturation on CO₂ storage in aquifers is one of the most important findings of this study. The simulations discussed above assume a single value of residual gas saturation for the entire aquifer. In general, this parameter will vary with rock type²⁸. For example, data suggest a correlation between residual gas saturation and porosity²⁹. To examine the implications of this variability, we conducted a second set of simulations with stochastic porosity/permeability realizations (Table 2). The porosity values for each block were then calculated using the following correlation²⁹

$$k = 7E \times 7 \phi^{9.606}$$

Based on the values of porosity for each grid, maximum residual gas saturation and residual water saturation values were found using following correlations²⁹

$$S_{gr}^{max} = 0.5473 - 0.9696 \phi$$

$$S_{wirr} = 5.6709 \times (\text{Log}(k) / \phi)^{-1.6349}$$

We also accounted for the fact that the relative permeability of the gas phase depends on whether it is displacing or being displaced by water. GEM models hysteresis with the following equations:

$$k_{rg}(S_g) = k_{rg}(\text{Drainage}; S_g) \text{ during drainage};$$

$$k_{rg}(S_g) = k_{rg}(\text{Drainage}; S_g(\text{shifted})) \text{ during imbibition};$$

where

$$S_g(\text{shifted}) = \frac{(S_g - S_{grh})(S_{gh})}{(S_{gh} - S_{grh})}$$

$$\text{and } \frac{1}{S_{gr}^{max}} - 1 = \frac{1}{S_{grh}} - \frac{1}{S_{gh}}$$

S_{gh} is the value of S_g when the shift to imbibition occurs

S_{grh} is the value of S_{gr} corresponding to S_{gh} via Land's equation

S_{gr}^{max} has the value of the user-entered parameter S_{gr}^{max}

In these simulations, a set of ten to fifteen intervals of porosity values was defined. Each interval was assumed to represent a single rock type and hence was assigned a different relative permeability curve and a different value of S_{gr}^{max} and S_{wirr} . The latter were calculated using the average porosity value for the interval. Figure 5 shows the correlation between different aquifer properties plotted with actual values used in simulations. An example relative permeability curve is shown in Figure 6.

To study the effect of the injector completion, CO₂ was injected only in the bottom half of the aquifer. Also, CO₂ was injected for 50 years, rather than 10 years, to investigate how the much larger volume of CO₂ would affect storage.

The simulations conducted with partial well completion in stochastic porosity/permeability realizations with hysteretic relative permeability and rock-type-dependent residual gas saturation indicate that with time all the gas will be trapped in various forms and will never reach the top seal of the aquifer. Figure 7 shows the gas injection profile at 50 years for a vertical x - z cross-section through the injector. Figure 8 shows the same profile after 1000 years. Figure 9 shows the CO₂ mole fraction in the aqueous phase while Figure 10 shows the H₂O mole fraction in the gas phase for the same cross-section after 1000 years.

Some 25% of the injected CO₂ exists as a mobile CO₂-rich gas phase at the end of the 50 year injection period. Figure 11 shows an important consequence of buoyancy-driven fluid movement after injection ends: CO₂ is transferred from the mobile phase into permanently stored forms. The time scale for this transfer depends strongly on aquifer properties, including dip; for this example the transfer is essentially complete within 1000 years. This simulation shows the benefit of CO₂ movement after injection ends, but this movement also presents a potential disadvantage. Figure 12 shows the gas saturation profile at 1000 years when CO₂ is injected through the entire interval of the well, rather than the bottom half. Migration of CO₂ updip along the top seal is evident. This result emphasizes the importance of engineering design in an aquifer storage scheme. A good understanding of the target formation, of the key physicochemical phenomena, and of classical reservoir engineering concepts will be prerequisite for ensuring long-term storage.

Influence of mineralization

To study the possible contribution of mineralization to CO₂ storage, we performed a third set of simulations in a one-dimensional tilted aquifer (1° dip) derived from the base case described above. This is shown schematically in Figure 13. The homogeneous horizontal permeability is 197.5 md and the porosity is 0.25. The reservoir temperature is 60 °C and the dispersion coefficient is 2×10^{-5} cm²/s. Salinity is 100,000 ppm. For simplicity, CO₂ solubility was modeled with Henry's law^{8,20} using a constant of 3.85×10^5 kPa. Relative permeability curves are shown in Figure 3 and capillary pressure is ignored.

The three aqueous reactions and five mineral reactions, described in Tables 4 and 5, were used in all simulations. The reaction equations for five the minerals are as follows:

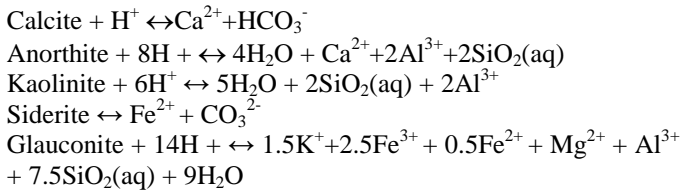


Table 6 shows the initial concentrations for aqueous components and the mineral properties and initial volume fractions are shown in Table 7. These mineral compositions are based on a glauconitic sandstone aquifer in the Alberta Sedimentary Basin, Canada^{4,8}.

In this example, we set the residual gas saturation to 0.25 and the initial gas saturation to be zero. Supercritical CO₂ is injected for 10 years with the rate of 100 m³/day. A production well is placed at each boundary to maintain constant far-field pressure. The total amount of CO₂ injection is 9.2×10⁹ gmol. Then we stop the CO₂ injection and continue the simulation for 10,000 years.

The average concentrations of calcite and siderite for Case 1 are shown in Figure 14. During the CO₂ injection period, the calcite initially present in the aquifer starts to dissolve because the dissolved CO₂ perturbs the initial aqueous phase composition so that it becomes undersaturated with respect to calcite. Since the average water saturation decreases during the first 10 years, mineral concentrations increase even though mineral dissolution occurs. Figure 14 shows that the mineralization (precipitation of calcite) starts after the injection stops. The siderite curve does not show significant responses after 10 years.

Anorthite and calcite average concentrations are presented on a linear time axis in Figure 15. The calcite concentration increases nonlinearly and stabilizes at 1.62×10³ gmol/kg water. Calcite precipitation requires a source of calcium cations, which provided in this example by the dissolution of anorthite. Thus the calcite precipitation is symmetric with the anorthite dissolution. Because very little fluid migration occurs after injection ends, the perturbation of the aqueous phase composition is limited to the region contacted by CO₂ during injection. This defines the mineralization region. The anorthite concentration in Figure 15 becomes constant when most of the anorthite in the mineralized region has dissolved, after 10000 years. In this example, 90.8% of injected CO₂ remains as a gas phase and 6.4% dissolves into water. About 2.7% of the CO₂ is mineralized into calcite. A relatively small amount of CO₂ stays as the bicarbonate ion (HCO₃⁻) and the amounts of the siderite precipitation and the carbonate ion are negligible. Even though the residual gas saturation is a modest 0.25, the residual saturation trapping is 46.8% and 44 % of total CO₂ is still mobile.

In the case described above (Case 1), we consider only CO₂ injection, and the majority of CO₂ remains in the gas phase. To evaluate the potential for reducing the amount of mobile gas in the aquifer, we simulated the injection of water simultaneously with the CO₂ injection (Case 2). We also simulated the injection of the same amount of the water as in Case 2, but immediately after the CO₂ injection (Case 3). As was mentioned previously, mineral precipitation depends highly on the amount and type of the source minerals, e.g., the

anorthite dissolution as a precursor for calcite precipitation. If we inject CO₂ in an anorthite-rich aquifer (Case 4), more calcite precipitation will occur. In Case 4, we increase the initial volume fraction of anorthite to 0.088, which is 10 times larger than Case 3, and the sequential water injection is also applied. Table 8 summarizes the formulation of simulation runs. The injection of water causes the gas saturation to decrease in the region around the injector because the CO₂ is displaced, and because the CO₂ remaining dissolves into water. Saturation fronts for Cases 1 and 2 are the same because the same amount of CO₂ is injected for 10 years for both cases. When CO₂ and water are injected sequentially, water pushes the gas saturation front and there is less mobile gas than the simultaneous injection case because CO₂ has more contact with the formation water. Only 10 % of injected CO₂ remains mobile after 10,000 years in Case 3.

Table 9 presents the CO₂ storage in various forms for each case at 10000 years. Even though the same amount of water is injected for Cases 2 and 3, more CO₂ dissolves into water when we apply the water injection sequentially. Owing to the large solubility of CO₂ in water, the injected water will dissolve out the residual gas phase saturation.

Figure 16 compares the calcite precipitation between Case 3 and 4. In Case 4, the calcite precipitation occupies 43.6 % of CO₂ for 70,000 years and keeps increasing thereafter. Compared with Case 3, about 22 % of CO₂ in gas phase is precipitated as calcite and the CO₂ dissolution in the aqueous phase is slightly decreased. If all the anorthite in the aquifer were converted to calcite, the theoretical potential of mineral trapping would be 46.2% of the injected CO₂.

Figure 16 shows that mineralization is negligible over the time scales considered in Figures 7 to 9, i.e. over the span of 1000 years. The fraction of injected CO₂ stored as calcite begins to increase after a few thousand years. The transfer of CO₂ from the gas phase to the mineral phase (mediated by the aqueous phase dissolution of anorthite) is limited by the rate of anorthite dissolution. Given enough time and a sufficient supply of calcium ion, however, this mechanism substantially decreases the amount of CO₂ stored as a mobile gas phase.

Conclusions

The concerns about CO₂ escape pathways from aquifers used for storage can be considerably mitigated if all or almost all of the CO₂ were stored in the immobile forms of residual gas, dense brine and minerals. We simulated CO₂ injection in deep, saline aquifers with emphasis on those mechanisms that would immobilize (store) the CO₂. The most significant conclusion from this scoping study is that the effect of residual gas on CO₂ storage can be very large, even more significant than storage in brine or minerals. Potentially all of the CO₂ can be stored in an immobile form when advantage is taken of this well-known phenomenon of capillary trapping. Therefore, the magnitude and variation of residual gas saturation as a petrophysical property merit further study. Both aquifer dip and horizontal to vertical permeability ratio have a significant effect on gas migration, which in turn affects CO₂ dissolution in brine and mineralization.

Well completions play an important role in deciding the fate of CO₂ after injection. When the supercritical CO₂ enters the aquifer near the top seal, it is likely to continue to migrate

up dip for long distances and thus may eventually find an escape path. On the contrary, when the CO₂ is injected in the bottom half of the aquifer, gravity-driven flow steadily reduces the amount of mobile gas before it can migrate to the top of the aquifer. The time scale for reduction of mobile gas to insignificant values strongly depends on the petrophysical parameters of the aquifer. Over the range of parameters investigated in this scoping study, very little mobile gas remained in the aquifer after a few hundred years.

For the cases studied, mineralization (conversion of dissolved CO₂ into carbonate minerals) occurs over a much longer time scale, on the order of 10⁴ years, primarily because of the slow reaction rates of the chemical reactions. However, if the rate of gravity-driven gas movement is sufficiently small, mineralization could play a significant role in immobilizing injected CO₂.

Injecting water after the CO₂ injection period increases the storage capacities of solubility and mineral trapping. The amount of the mobile gas phase drops significantly because the gas phase is displaced by the injected water and spreads out. This effect would be attenuated if the injected water were saturated with CO₂.

For the cases studied here, the capacity of CO₂ storage by mineral trapping is relatively small compared to residual saturation trapping or mobile gas. The amount of minerals containing divalent cations initially present in the aquifer, and the rate at which they dissolve, control the relative amounts of carbonate minerals precipitated.

Acknowledgement

This research was supported by fellowships and grants from the National Energy Technology Laboratory of the U.S. Department of Energy and the CO₂ Capture Program. We especially wish to thank Duane Smith at NETL for his support of the initial CO₂ research by Vikas and A. Kumar at UT as part of their MS theses. We also want to thank CMG Ltd. for making available the GEM simulator used in this research. Larry W. Lake holds the W. A. (Monty) Moncrief Centennial Chair, Kamy Sepehrnoori holds the Bank of America Centennial Professorship and Gary A. Pope holds the Texaco Centennial Chair at The University of Texas at Austin.

Nomenclature

k	permeability, md
k _{rg}	gas relative permeability
k _{rw}	water relative permeability
S _g	gas saturation, fraction
S _{gr} ^{max}	maximum residual gas saturation, fraction
S _{wirr}	irreducible water saturation, fraction

Greek Symbols

φ	porosity
---	----------

References

1. Pruess, K., Xu, T., Apps, J., and Garcia, J., "Numerical Modeling of Aquifer Disposal of CO₂," SPE Journal, SPE 83695, pp 49-60, March 2003.
2. Bachu, S., Gunter, W. D., and Perkins, E. H., "Aquifer Disposal of CO₂: Hydrodynamic and Mineral Trapping," *Energy Conversion and Management*, Vol 35, pp 269-279, 1994.
3. Doughty, C., and Pruess, K., "Modeling Supercritical CO₂ Injection in Heterogeneous Porous Media," paper presented at TOUGH Symposium, California, May 2003.
4. Gunter, W. D., Wiwchar, B., and Perkins, E. H., "Aquifer Disposal of CO₂-rich Greenhouse Gases: Extension of the Time Scale of Experiment for CO₂ - Sequestering Reactions by Geochemical Modeling," *Mineralogy and Petrology*, Vol 59, pp121-140, 1997.
5. Hichon, B., Gunter, W. D., and Gentzis, T., "The Serendipitous Association of Sedimentary Basins and Greenhouse Gases," Proceedings, American Chemical Society Symposium on CO₂ capture, utilization and disposal Orlando, Florida, pp 25-29, 1996.
6. House, N.J., Faulder, D.D., Olson, G.L., and Fanchi, J.R., "Simulation Study of CO₂ Sequestration in a North Sea Formation," paper SPE 81202 presented at the SPE/EPA/DOE Exploration and Production Environmental Conference, San Antonio, March 2003.
7. King J.E., "Role of Convective Mixing in the Long-Term Storage of Carbon Dioxide in Deep Saline Formations," paper SPE 84344 presented at SPE Annual Technical Conference and Exhibition, October, 2003.
8. Nghiem, L., "Compositional Simulator for Carbon Dioxide Sequestration," Computer Modeling Group Ltd., 2002.
9. Pasala, S.M., Forster, C.B., Lim, S.J., and Deo, M.D., "Simulating the Impact of Faults on CO₂ Sequestration and Enhanced Oil Recovery in Sandstone Aquifers," paper SPE 84186 presented at the SPE Annual Technical Conference and Exhibition, Denver, October 2003.
10. Pruess, K., Bielinski, A., Ennis-King, J., Fabriol, J., Gallo, Y.L., García, J., Jessen, K., Kovscek, T., Law, D.H.S., Lichtner, P., Oldenburg, C., Pawar, R., Rutqvist, J., Steefel, C., Travis, B., Tsang, C.F., White, S., Xu, T., "Code Intercomparison Builds Confidence in Numerical Models for Geologic Disposal of CO₂," <http://www-esd.lbl.gov/GEOSEQ/index.html>.
11. Seo, J.G., and Mamora, D.D., "Experimental and Simulation Studies of Sequestration of Supercritical Carbon Dioxide in Depleted Gas Reservoirs," paper SPE 81200 presented at the SPE/EPA/DOE Exploration and Production Environmental Conference, San Antonio, March 2003.
12. Xu, T., Apps, J. A., and Pruess, K., "Analysis of Mineral Trapping for CO₂ Disposal in Deep Aquifers," Berkeley, California: Lawrence Berkeley Natl. Lab. Rep. LBNL-46992, 2001.
13. Vikas, "Simulation of CO₂ Sequestration," MS thesis, University of Texas at Austin, 2002.

14. Wellman, T. P., Grigg, R. B., McPherson, B.J., Svec, R.K., and Lichtner, P.C., "Evaluation of CO₂-Brine-Reservoir Rock Interaction with Laboratory Flow Tests and Reactive Transport Modeling," paper SPE 80228 presented at the SPE International Symposium on Oilfield Chemistry, Houston, February 2003.
15. Rumpf, B., Nicolaisen, H., Ocal, C. and Maurer, G.(1993). "Solubility of Carbon Dioxide in Aqueous Solutions of Sodium Chloride: Experimental Results and Correlation," *Journal of Solution Chemistry*, Vol. 23, No.3, pp 431-438, 1994.
16. Scharlin, P., "Carbon Dioxide in Water and Aqueous Electrolyte Solutions," volume 62 of Solubility Data Series. Oxford University Press, International Union of Pure and Applied Chemistry, Oxford, UK, 1996.
17. Spycher, N., Pruess, K., Ennis-King, J., "CO₂-H₂O Mixtures in the Geological Sequestration of CO₂. I. Assessment and Calculation of Mutual Solubilities from 12 to 100 °C and up to 600 bar," Lawrence Berkeley National Laboratory, report LBNL- 50991, July 2002.
18. Teng, H. and Yamasaki, A., "Solubility of Liquid CO₂ in Synthetic Sea Water at Temperatures from 278 K to 293 K and Pressures from 6.44 MPa to 29.49 MPa, and Densities of the Corresponding Aqueous Solutions," *Journal of chemical & engineering data*, Vol 43, pp 2-5, 1998.
19. Teng, H., Yamasaki, A., Chun, M. K. and Lee, H., "Solubility of Liquid CO₂ in Water at Temperatures from 278 K to 293 K and Pressures from 6.44 MPa to 29.49 MPa and Densities of the Corresponding Aqueous Solutions," *Journal of chemical & engineering data*, Vol 29, pp 1301-1310, 1997.
20. Li, Y. K. and Nghiem, L. X., "Phase Equilibria of Oil, Gas and Water/Brine Mixtures from a Cubic Equation of State and Henry's Law," *Can. J. Chem. Eng.* 64, pp 486-496, 1986.
21. Firoozabadi, A., Nutakki, R., Wong, T.W., and Aziz, K., "EOS Predictions of Compressibility and Phase Behavior in Systems Containing Water, Hydrocarbons, and CO₂," *SPE Reservoir Engineering*, SPE 15674, Vol 3, No. 2, May 1988.
22. Garcia, J. E., "Density of Aqueous Solutions of CO₂," Lawrence Berkeley National Laboratory, report LBNL-49023, October 2001.
23. Grigg, U., Straub, J., Schiebener, P., *Steam Tables in SI-Units*, Springer-Verlag, Third Edition, 1990.
24. Hnědkovský, L., Wood, R. H., and Majer, V., "Volumes of Aqueous Solutions of CH₄, CO₂, H₂S and NH₃ at Temperatures from 298.15 K to 705 K and Pressures to 35 Mpa," *Journal of Chemical Thermodynamics*, Vol 28, pp 125-142, 1996.
25. Simonson, J. M., Oakes, C. S. and Bodnar, R. J., "Densities of NaCl(aq) to the Temperature 523 K at Pressures to 40 MPa Measured with a New Vibrating-tube Densitometer," *Journal of Chemical Thermodynamics*, Vol 26, pp 345-359, 1994.
26. Wagner, W. and Průš, A., "The IAPWS Formulation 1995 for the Thermodynamic Properties of Ordinary Water Substance for General and Scientific Use," *J. Phys. Chem. Ref. Data*, Vol. 31, No. 2, pp 387-535, 2002.
27. Zaytsev, I. D., and Aseyev, G. G., "Properties of Aqueous Solutions of Electrolytes," CRC Press.
28. Parkinson, W. and Nevers, N. D., "Partial Molal Volume of Carbon Dioxide in Water Solutions," *Industrial and Engineering Chemistry Fundamentals*, Vol. 8, No. 4, pp 709-713, 1969.
29. Lake, L. W., *Enhanced oil recovery*, New Jersey: Prentice Hall, 1989.
30. Holtz, H. M., "Residual Gas Saturation to Aquifer Influx: A Calculation Method for 3-D Computer Reservoir Model Construction," paper SPE 75502 presented at SPE Gas Technology Symposium, April– May 2002.

SI Metric Conversion Factors

$$\begin{aligned} \text{ft} \times 3.048\text{E-1} &= \text{m} \\ \text{psi} \times 6.894757 &= \text{KPa} \\ \text{lb/ft}^3 \times 1.601846\text{E1} &= \text{kg/m}^3 \\ \text{ft}^3/\text{lb-mole} \times 6.242796\text{E-5} &= \text{m}^3/\text{g-mole} \end{aligned}$$

Table 1: Simulation Input for Base Case Simulation

<i>Aquifer Properties</i>		
Length, ft	53000	
Width, ft	53000	
Thickness, ft	1000	
Depth at top of formation at injection well, ft	5300	
Temperature, °F	140	
Initial pressure, psia	2265	
Dip, degree	1	
Salinity, ppm	100000	
Dykstra-Parsons coefficient	0.7	
Horizontal to vertical permeability ratio	0.001	
Mean permeability, md	100	
Horizontal permeabilities of each layer*, md		
Layers 1-4	89	
Layers 5-8	65	
Layers 9-12	46	
Layers 13-16	30	
Layers 17-20	15	
Layers 21-24	120	
Layers 25-28	165	
Layers 29-32	235	
Layers 33-36	840	
Layers 37-40	370	
Porosity	0.25	
Residual water saturation	0.25	
Residual gas saturation	0.25	
Gas end point relative permeability	1.0	
Water end point relative permeability	0.334	
Grid	40x40x40	
Maximum injection pressure, psia	3300	
Maximum injection rate, MMSCF/D	50	
<i>Description of Components</i>		
<u>Component</u>	<u>CO₂</u>	<u>H₂O</u>
Critical pressure, psi	1070.0	3200.11
Critical temperature, °F	87.77	705.1
Critical volume, cu ft/lb-mole	1.5076	0.8962
Molecular weight, lb/lb-mole	44.01	18.015
Acentric factor, dimensionless	0.22394	0.344
Parachor, dimensionless	78	52

*Layer 1 is the top layer.

Table 2: Summary of Simulations Made for Sensitivity Analysis

Parameter Varied	Results/Comments
<i>Layered permeability (Injection for 10 years)</i>	
(Base case)	
Temperature = 110 °F Temperature = 140 °F* Temperature = 170 °F Temperature = 200 °F Temperature = 230 °F	Increase in temperature leads to increased dissolution of gas into brine
Mean permeability = 10 md Mean permeability = 100 md* Mean permeability = 1000 md	Increase in mean permeability leads to greater injectivity as well as greater migration of CO ₂
Salinity = 0 ppm Salinity = 50,000 ppm Salinity = 100,000 ppm* Salinity = 200,000 ppm Salinity = 300,000 ppm	Increase in salinity leads to decreased dissolution of gas into brine
Kv/Kh = 0 Kv/Kh = 0.001* Kv/Kh = 0.01 Kv/Kh = 0.1 Kv/Kh = 1	Increase in Kv/Kh value leads to upward migration of gas and finally its migration along seal
S _{gr} = 0.05 S _{gr} = 0.15 S _{gr} = 0.25* S _{gr} = 0.35 S _{gr} = 0.5	Low value for S _{gr} leads to increased gas migration and dissolution in brine, while high value leads to increased trapping as residual gas
Dip = 0° Dip = 1° * Dip = 2.5° Dip = 5°	Increase in dip leads to increased gas migration and dissolution into brine
<i>Stochastic Permeability (Injection for 50 years)</i>	
(Stochastic permeability base case)**	
Mean permeability** = 10 md (other properties correlated) Mean permeability** = 1000 md (other properties correlated)	Increase in mean permeability leads to increased injectivity and dissolution into brine

*Base Case

**Correlation lengths: Δx = Δy = 5000ft, Δz = 50ft

Table 3: Experimental Data for CO₂-Solubility in Brine

Source	Temperature Range, °F	Pressure Range, psia	Salinity Range, ppm total dissolved solids
15	104-319	100-1400	230,000-350,000
16	120-302	1450-5800	0
18-19	40-69	930-4280	0-31,000

Table 4: Aqueous Reactions

Reaction	Equilibrium Constant, log ₁₀ K
H ₂ O ↔ H ⁺ + OH ⁻	-13.2631
CO ₂ (aq) + H ₂ O ↔ H ⁺ + HCO ₃ ⁻	-6.3221
CO ₂ (aq) + H ₂ O ↔ 2H ⁺ + CO ₃ ²⁻	-16.5563

Table 5: Mineral Reactions

Mineral	Log ₁₀ K _{sp}	Log ₁₀ k _β , mol/m ² -s	Ĥ _β , m ² /m ³	E _{aβ} , J/mol
Calcite	1.36	-8.8	88	41870
Anorthite	-8	-12	88	67830
Kaolinite	5.47	-13	17600	62760
Siderite	10.7	-9.35	88	41870
Glauconite	-8.6	-14	4400	58620

Table 6: Initial Concentrations for Aqueous Components

Aqueous Species	Concentration, mol/kg H ₂ O
H ⁺	1.0E-7
Ca ²⁺	9.12E-5
SiO ₂ (aq)	2.35E-8
Al ³⁺	2.32E-11
Fe ²⁺	3.22E-6
Fe ³⁺	4.99E-5
Mg ²⁺	5.E-7
K ⁺	5.E-7
OH ⁻	5.46E-7
CO ₃ ²⁻	2.49E-2
HCO ₃ ⁻	1.17E-5

Table 7: Mineral Properties

Mineral	Molecular Weight	Density, kg/m ³	Initial Volume Fraction
Calcite	100.1	2710	0.0088
Anorthite	278.2	2740	0.0088
Kaolinite	258.16	2410	0.0176
Siderite	115.86	3960	0.0088
Glauconite	426.93	2670	0.044

Table 8: Summary of Simulations With Mineral Reactions

Case 1 - CO ₂ injection only	Injection 100 m ³ /day of CO ₂ for 10 years and shut-in
Case 2 - simultaneous water injection	Co-injection 100 m ³ /day of CO ₂ and 100 m ³ /day of water for 10 years and shut-in
Case 3 - sequential water injection	Sequential injection 100 m ³ /day of CO ₂ for 10 years, then 100 m ³ /day of water for another 10 years and shut-in
Case 4	Increase initial anorthite concentration to 10 times more than that of Case 3

Table 9: Distribution [%] of Injected CO₂ for Test Cases at 10000 Years

	Gas		Aqueous	HCO ₃ ⁻	Calcite
	Mobile	Immobile			
Case 1	44.0	46.8	6.4	0.1	2.7
Case 2	31.9	55.2	9.4	0.1	3.4
Case 3	10.0	70.6	14.7	0.2	4.5
Case 4 (70,000 yrs)	2.7	43.3	10.3	0.1	43.6

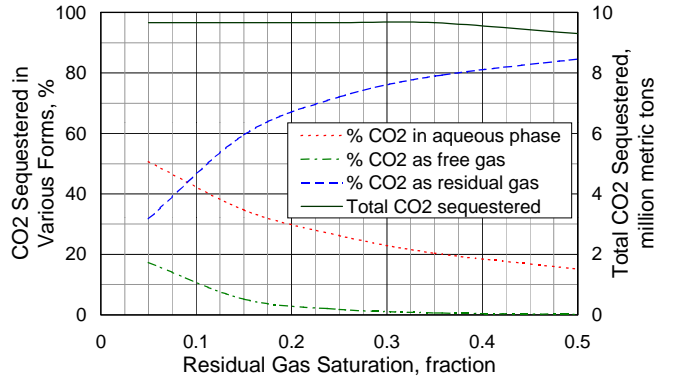


Fig. 4—Effect of residual gas saturation on the distribution of CO₂ between phases at 1000 years

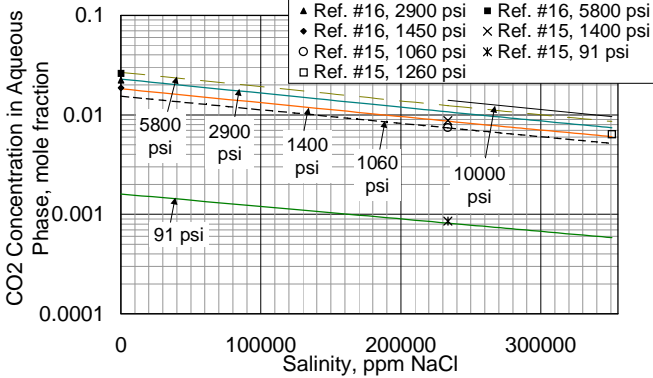


Fig. 1—Effect of brine salinity on CO₂ solubility in the aqueous phase at 140 °F (60 °C)

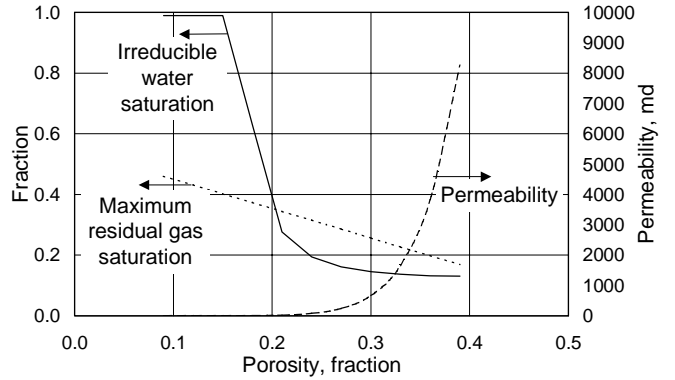


Fig. 5—Correlation between different aquifer properties³⁰

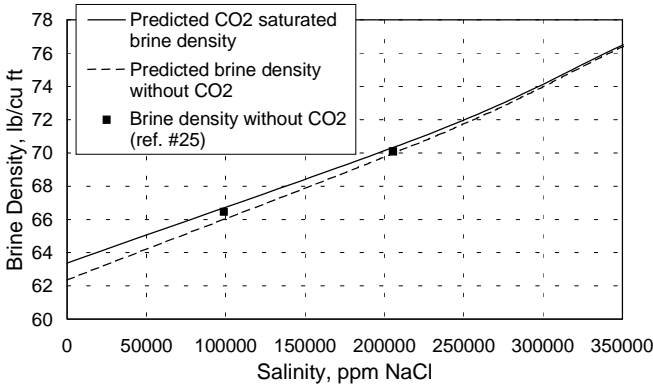


Fig. 2—Effect of CO₂ on brine density at 122 °F and 5830 psi

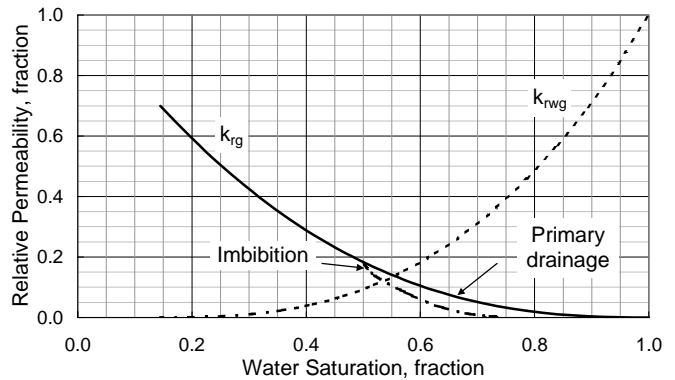


Fig. 6—Water-gas relative permeability curves with hysteresis

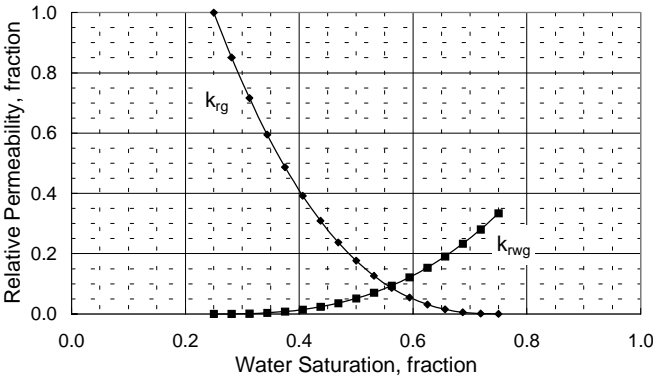


Fig. 3—Water-gas relative permeability curves

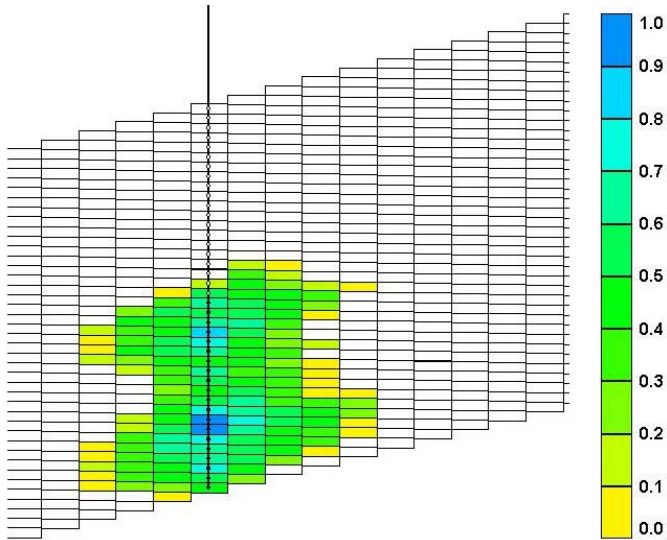


Fig. 7—Gas saturation at 50 years (zoomed-in vertical slice through the injection well in x-z direction)

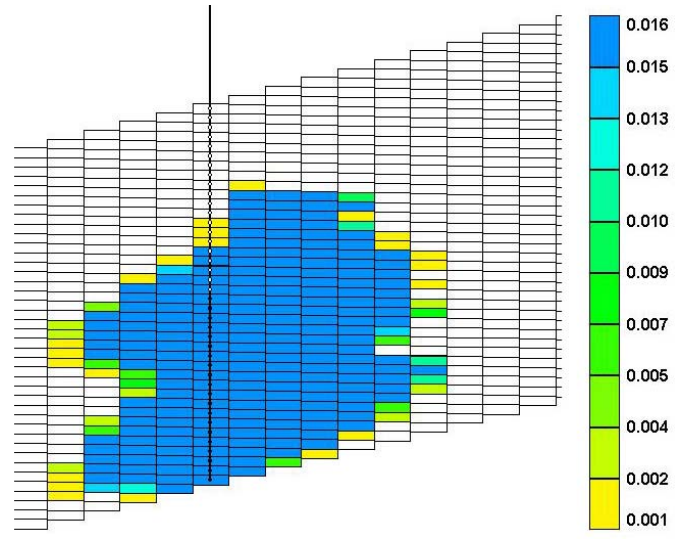


Fig. 9—CO₂ mole fraction in aqueous phase at 1000 years (zoomed-in vertical slice through the injection well in x-z direction)

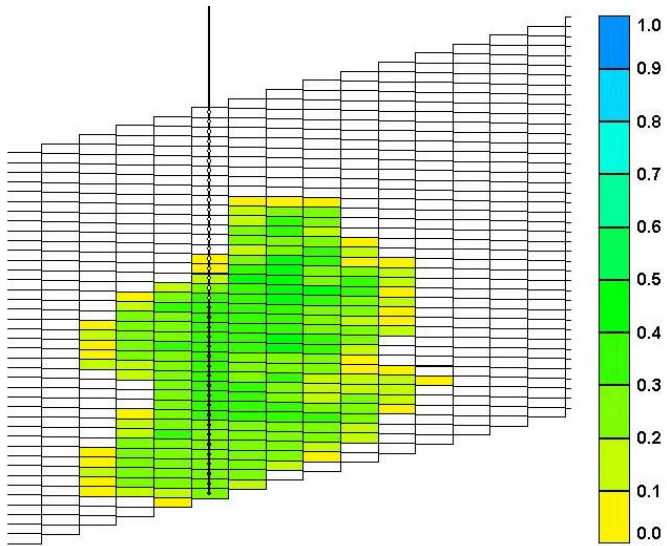


Fig. 8—Gas saturation at 1000 years (zoomed-in vertical slice through the injection well in x-z direction)

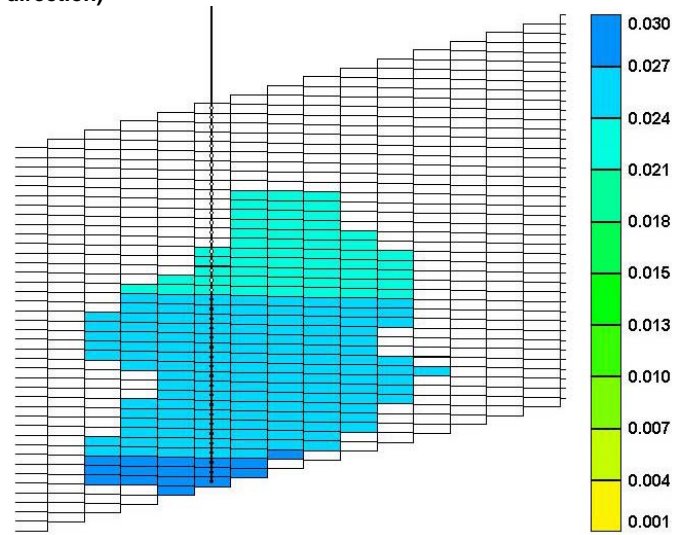


Fig. 10—H₂O mole fraction in gas phase at 1000 years (zoomed-in vertical slice through the injection well in x-z direction)

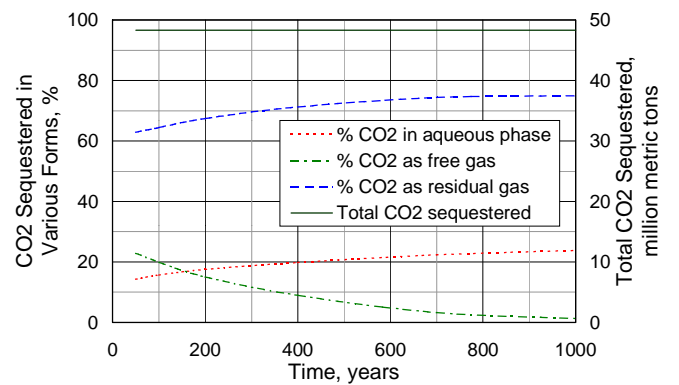


Fig. 11—Effect of gravity-driven fluid migration on the distribution of CO₂ between phases after injection for 50 years (at 1000 years)

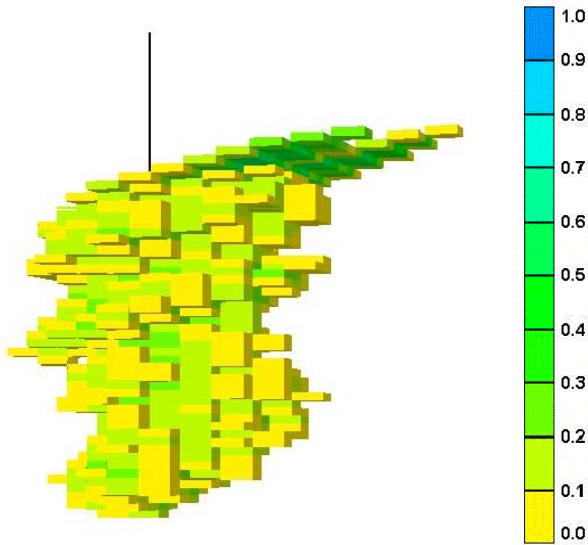


Fig. 12—3-D Gas saturation profile at 1000 years for injection along whole interval

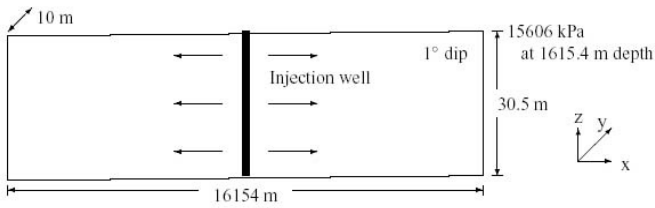


Fig. 13—Schematic of 1D flow field used for simulations that account for mineralization

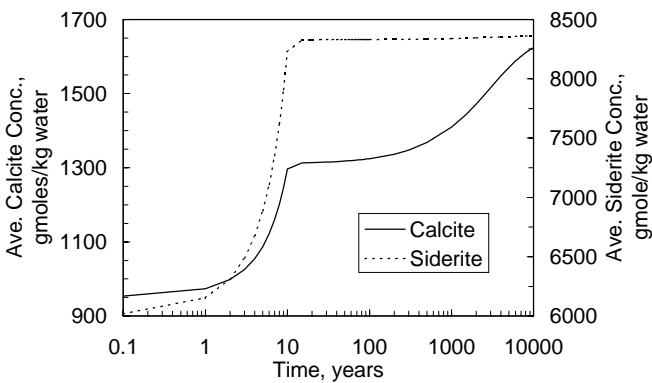


Fig. 14—Mineral concentrations for Case 1

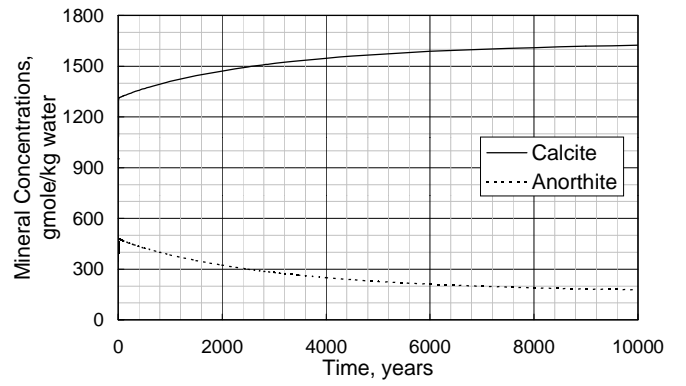


Fig. 15—Concentration history of anorthite and calcite for Case 1

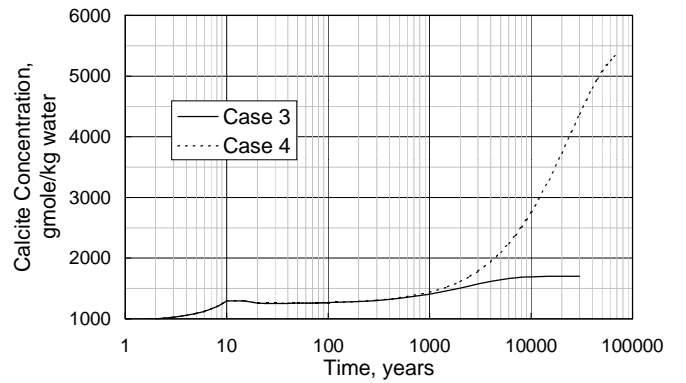


Fig. 16—Comparison of calcite precipitation histories for Case 3 and 4. Case 4 has 10 times more initial anorthite than Case 3